Structure and Electronic and Charge-Transfer Properties of Mercaptobenzoic Acid and Mercaptobenzoic Acid−Undecanethiol Mixed Monolayers on Au(111)

Miriam C. Rodríguez González,[†] Alejandro González Orive,[†] Pilar Carro,[†] Roberto C. Salvarezza,[‡] and Alberto Hernández Creus[†,*]

[†]Área de Química Física, Departamento de Química, Facultad de Ciencias, Universidad de La Laguna, Instituto de Materiales y Nanotecnología, Avda. Francisco Sánchez s/n, 38071-La Laguna, Tenerife Spain

[‡]Instituto de Investigaciones Fisicoquímicas Teóricas y Aplicadas (INIFTA), Universidad Nacional de La Plata - CONICET, Sucursal 4 Casilla de Correo 16, (1900) La Plata, Buenos Aires, Argentina

ABSTRACT: The surface structure, molecular conductance, and charge-transfer properties of pure mercaptobenzoic acid (MBA) and mixed MBA−undecanethiol (UDT) self-assembled monolayers (SAMs) on Au(111) are studied by scanning tunneling microscopy, scanning tunneling spectroscopy, electrochemical techniques, and density functional theory calculations. MBA forms ordered diluted lattices without evidence of Au adatom complexes at terraces (absence of vacancy islands) at low MBA concentrations, whereas disordered lattices with possible formation of these complexes are found at high concentrations (presence of vacancy islands). In addition, some other interesting facts have been established.

The stability of the MBA SAMs is improved in mixed MBA−UDT SAMs, revealing aromatic−aliphatic attractive interactions. The mixed SAMs at equivalent amounts of thiols hinder the vacancy island formation typical of the pure UDT SAMs. The MBA SAMs exhibit good molecular conductance with filled states from S and aromatic ring contributions near the Fermi level. Finally, it has been proven that MBA molecules efficiently wire the electron transfer through UDT SAMs.
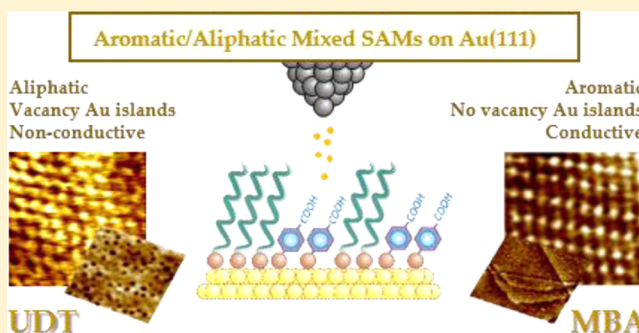
1. INTRODUCTION

Self-assembled monolayers (SAMs) have been established as essential systems in surfaces modification and functionalization because of their huge potential in many applications, especially in nanoscience and nanotechnology fields.[1−4] Some of these applications include biosensors, corrosion protection, wetting control, drug delivery systems, and molecular devices.[5,6]

In most cases, single-component monolayers have been studied. However, in recent years the number of studies focused on designing and controlling surface properties with mixed SAMs have increased, especially those composed by species with a different structure or functional groups.[7,8] Many methodologies of preparing binary SAMs have been reported, including replacement of absorbed thiols,[9] electrochemical control of adsorption,[10] and selective electrochemical desorption of a monolayer followed by readsorption.[11] The most common method of forming a SAM composed by two species consists of coadsorption from a solution containing two components onto the surface or ligand replacement after a pure SAM is prepared.[7,8]

Commonly, the presence of a SAM in a surface is determined by using electrochemical techniques. Using cyclic voltammetry, the formation of a binary SAM can be checked. When a voltammogram of a binary SAM is studied, two different cases

can be found. If very similar thiols are used for the formation of the binary SAM, only one desorption peak is found in the voltammogram, related to the binary SAM. In this case, the SAM consists of a homogeneous mix of the thiols employed. This situation occurs when the difference between the desorption potentials of similar thiols is less than 0.20 V.[12] Nevertheless, the most common situation is the presence of two electrodesorption peaks where desorption potentials are different from those of the pure SAMs. In general, the potential peak of the less stable thiol appears at more negative values because of the incorporation of molecules of the more stable thiol, forming a domain rich in the first one, but not pure.[13,14] Using this technique combined with scanning tunneling microscopy (STM), X-ray photoelectron spectroscopy (XPS), or Raman spectroscopy, considerable knowledge about these SAMs has been obtained.[15,16] Thus, the spatial distribution of thiols in binary SAMs can be described by two different situations: a phase separation structure for thiols with different lengths[13,17] and randomly mixed structure for thiols of comparable lengths.[12] These results show that the degree of

different lengths of thiols composing the binary SAMs influences the spatial distribution of the species.[18]

In this work we have used two very different thiols to form mixed SAMs to obtain key information about thiolate organization on the Au(111) surface. Thus, we have mixed 4-mercaptobenzoic acid (MBA), a small, conductive, and non-vacancy Au island-forming aromatic thiol, and undecanethiol (UDT), a long, non-conductive, and vacancy island-forming aliphatic thiol. Vacancy islands have been taken as a fingerprint for Au(111) reconstruction by the formation of Au_{ad}-thiolate complexes (Au_{ad}-SR). The presence or absence of vacancy islands as a function of UDT/MBA surface coverage could give information about the process of Au(111) reconstruction and Au_{ad}-SR complex formation. In addition, the mixed SAMs can help us to understand aromatic–aliphatic thiolate interactions at surfaces and the conductive properties of aromatic and aliphatic molecules. The methodology used in this work includes cyclic voltammetry, STM, and scanning tunneling spectroscopy (STS) complemented with density functional theory (DFT) calculations.

2. EXPERIMENTAL SECTION

2.1. SAM Formation. 4-Mercaptobenzoic acid (MBA) (Aldrich, 99%), undecanethiol (UDT) (Aldrich, 98%), NaOH (Merck, 99%), absolute ethanol (Panreac, 99.5%), potassium ferrocyanide (Merck), and potassium ferricyanide (Merck) were used as received. Evaporated Au on chromium-coated glass plates (Arrandee) was used as substrates. Theses plates, after flame annealing, consist of micrometer-sized Au(111) preferred-oriented single crystals with atomically smooth triangular terraces separated by monatomic steps in height. The height of these steps (0.24 nm) is revealed by STM.

Pure MBA SAMs were formed on the Au(111) substrates by using immersion times (t) from 1–2 h to 24–72 h of the clean substrates in 10^{-4}–10^{-2} M MBA ethanolic solutions. After that, the samples were removed from the solution, rinsed with ethanol, and dried under N_2. Pure UDT SAMs were formed by immersion overnight of the substrate in a 10^{-4} M solution. Then, the samples were rinsed with ethanol and dried for further investigation. Simultaneous adsorption of both thiols for the formation of mixed SAMs was performed by immersing the substrate for 1 h in an ethanolic solution containing the thiols in a strictly controlled ratio. Concentration for UDT was fixed at 10^{-4} M, and MBA concentration was increased from 10^{-4} to 10^{-2} M to obtain different UDT/MBA ratios.

2.2. Scanning Tunneling Microscopy and Scanning Tunneling Spectroscopy. Topographic STM images (constant current mode) were taken with a Nanoscope IIE (from Digital Instrument/Bruker) operating in air at room temperature using commercial Pt/Ir and electrochemically etched W tips. Tunneling current (i_t) and applied bias voltage (V_{bias}) to obtain good quality images were 0.15–0.3 nA and −0.6 to +1 V, respectively, at scan rates in the 0.5–10 Hz range. Some of the images were analyzed by using WSxM software.[19] The scanner calibration was checked by imaging highly oriented pyrolytic graphite (HOPG) with atomic resolution.

The i_t versus V_{bias} curves were averaged over at least three different regions of the samples. In STS measurements positive bias means that the sample is made positive. The di_t versus dV_{bias} (tunneling conductance) plots shown in this paper are the average of at least 200 tunneling i_t versus V_{bias} curves obtained in different zones of the sample under the same experimental conditions. In the measurements, V_{bias} was

scanned between 2 and −2 V, and it should be noted that these limits cannot be extended because of the loss of SAM integrity.

2.3. Electrochemical Measurements. Cyclic voltammetry was performed with a Autolab PGSTAT30 potentiostat and a three-electrode cell using the thiol-modified Au(111) substrate as working electrode, a large area Pt plate as counter electrode, and a Ag/AgCl as reference electrode mounted in a conventional glass cell. All the potentials in the text are referred to the reference electrode scale. Aqueous 0.1 M NaOH solutions were prepared by using deionized H_2O from a Milli-Q purification system (Millipore Products), which were degassed with purified nitrogen prior to the experiments. Thiol reductive electrodesorption was performed by scanning the potential from −0.3 to −1.4 at 0.05 V s^{-1} in the 0.1 M NaOH solution at room temperature. In each case, the charge density (q) involved in the reductive peak desorption was calculated by integration of the peak area. The total electrode real area was measured through the gold oxide reduction peak after the complete electrodesorption of the thiol. This figure was taken as an indication of the surface coverage by the thiol SAM. The q values for each SAM resulted from an average of at least 20 electrodesorption curves.

To check the blocking properties of the pure and mixed SAMs, the electrochemical response of the $[Fe(CN)_6]^{4-}$/$[Fe(CN)_6]^{3-}$ redox couple was used. To this end, an aqueous solution of 1 mM $K_4[Fe(CN)_6]$/$K_3[Fe(CN)_6]$ in 0.1 M KNO_3 was employed. In this case, cyclic voltammetry was performed by scanning the potential from −0.25 to 0.8 at 0.01 V s^{-1}.

2.4. Computational Methods. Calculations for MBA structural models on the Au(111) surface were performed by using the periodic plane-wave set code Vienna Ab initio simulation package (VASP 5.2.12) based on density functional theory (DFT).[20,21] We have followed the scheme of nonlocal functionals proposed by Dion et al.,[22] vdW-DF, and the optimized Becke88 exchange functional optB88-vdW[23] to take into account the van der Waals (vdW) interactions. The electronic wave functions were expanded in a plane-wave basis set with a 450 eV cutoff energy. The Blöchl projector augmented plane wave (PAW) method has been used to represent the atomic cores[24] with PBE potential. Gold surfaces were represented by five atomic layers, and a vacuum of ~12 Å separates any two successive slabs. Optimal grids of Monkhorst–Pack[25] k-points 9 × 4 × 1 and 5 × 4 × 1 have been used for numerical integration in the reciprocal space of ($\sqrt{3}$ × 4) and c(4 × 2) surface structures, respectively. Surface relaxation is allowed in the three uppermost Au layers of the slab, and the atomic coordinates of the adsorbed species were allowed to relax without further constraints. The atomic positions were relaxed until the force on the unconstrained atoms was less than 0.03 eV/Å. The adsorbates are placed on only one side of the slab, and all calculations include a dipole correction. Radical species (RS*) for MBA was optimized in an asymmetric box of 20 × 20 × 40 Å^3. The calculated Au lattice constant is 4.16 Å, which compares reasonably well with the experimental value (4.078 Å).[26]

The average binding energy per adsorbed MBA* radical, which results when MBA loses the hydrogen atom of the S−H group on Au(111) surface, E_b, is defined in eq 1

$$E_b = \frac{1}{N_{MBA*}}[E^{MBA*/Au} - E_{Au(111)}^R - N_{MBA*}E_{MBA*}] \tag{1}$$

where $E^{MBA*/Au}$, $E_{Au(111)}^R$, and E_{MBA*} stand for the total energy of the adsorbate−substrate system, the energy of the Au slab when MBA* moieties are removed, and the energy of MBA* radical, respectively, whereas N_{MBA*} is the number of MBA* radicals in the surface unit cell. A negative number indicates that adsorption is exothermic with respect to the separate clean surface and MBA* radical.

The possibility of a MBA lattice transition from diluted to the denser lattices on reconstructed Au(111) has been evaluated by using the Gibbs free energy of adsorption ($\gamma(\Delta\mu)$) defined as

$$\gamma(\Delta\mu_{MBA*}) \approx \frac{1}{A}[E^{MBA*/Au} - N_{Au}E_{Au}^{bulk} - N_{MBA*}\Delta\mu_{MBA*}] - \gamma_{clean}^U$$

$$\approx \frac{N_{MBA*}}{A}\left[E_b^{(MBA)_2} + \frac{E_{rec}}{N_{MBA*}}\right] + \gamma_{clean}^U - \frac{N_{MBA*}}{A}\Delta\mu_{MBA*}$$

(2)

as a function of the chemical potential ($\Delta\mu_{MBA*}$), where $E_b^{(MBA)_2}$ represents the binding energy per MBA* calculated with respect the total energy of gas phase (MBA)$_2$; A is the area of the surface unit cell, and γ_{clean}^U is the Gibbs free energy of the unreconstructed Au(111) surface. On the other hand, the reconstruction energy per unit cell for the different surfaces has been calculated as

$$E_{rec} = E_{Au(111)}^R - E_{Au(111)}^U - n_{ad}E_{bulk}^{Au}$$

where $E_{Au(111)}^R$ and $E_{Au(111)}^U$ correspond to the energy of reconstructed Au(111) surface and unreconstructed Au(111) surface per cell unit, respectively; E_{bulk}^{Au} is the total energy of a bulk Au atom, and n_{ad} is the number of Au adatoms in the surface unit cell. This energy is related to the Au adatom formation, which yields the RS-Au$_{ad}$-RS moieties.

3. RESULTS AND DISCUSSION

3.1. Pure SAMs. *3.1.1. MBA SAMs.* The electrodesorption curve for MBA SAMs formed by immersion of the Au(111) substrate in 10^{-4} M for 1 h is shown in Figure 1a. The main cathodic current peak appears at E_p= −0.61 V involving a
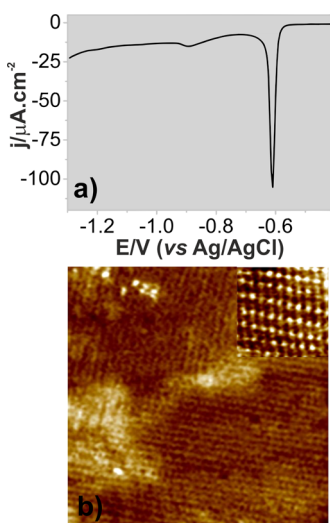
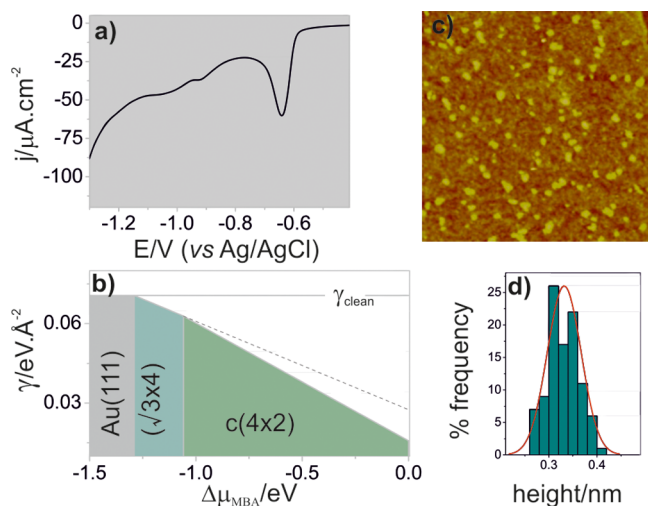**Figure 1.** MBA SAM, θ_{MBA}= 0.25. (a) Electrodesorption curve and (b) (25 × 25 nm^2) STM high-resolution image corresponding to MBA SAM formed by immersion of the Au(111) substrate in 10^{-4} M MBA ethanolic solution for 1 h. The inset in panel b (5 × 5 nm^2) shows the ($\sqrt{3}$ × 4) MBA lattice on Au(111).

charge density $q = 55.5\ \mu C\ cm^{-2}$.[27] This figure corresponds to a MBA surface coverage θ_{MBA}= 0.25, assuming one electron-transfer process. Moreover, two smaller peaks at −0.91 and −1.03 V can be observed as well, although this last peak is not always present and it has been assigned to MBA molecules absorbed on surface defects such as steps. Similar results have been obtained for 4-methylbenzenethiol (MBT)[28] with the main desorption peak taking place at E_p = −0.58 V and the smallest one at −0.91 V.

Figure 1b corresponds to *in air* STM image (25 × 25 nm^2) of MBA SAM on Au(111) showing ordered MBA domains formed by rows of bright spots. The periodic structure has been better defined in the higher-resolution image shown in the inset. This thiol lattice has been previously reported for MBA on the Au(111) surface in terms of a ($\sqrt{3}$ × 4) unit cell[27,29] and also for other aromatic thiols, such as MBT.[28] As already reported there are no vacancy islands on the STM images, in agreement with previous data on 4-mercaptophenol,[30] which could justify the formation of RS-Au$_{ad}$-SR species. In fact, vacancy islands usually present in alkanethiolate SAMs could be formed by gold atom removal from the topmost layer of the Au(111) to form RS-Au$_{ad}$-RS moieties, thus leaving on the Au terraces monatomic vacancies that yield the larger vacancy islands by Ostwald ripening. Contradictory results have been reported concerning the effect of thiol molecule size on vacancy island formation. In fact, there is some evidence that they do not form for short chain alkanethiols,[3,31,32] although other experimental results show that they are present in SAMs of ethanethiol,[33] propanethiol,[34] and butanethiol.[35] Our results reveal another interesting aspect of this process because for the same thiol it depends on the surface coverage. Thus, we consider that the ($\sqrt{3}$ × 4) MBA lattice is formed by RS* species, although we can not exclude the presence of some amount of RS-Au$_{ad}$-SR complexes formed by the reaction of MBA molecules with the Au$_{ad}$ provided by lifting of the herringbone reconstruction of the Au(111) after thiol adsorption. On the other hand, the fact that MBA and MBT have the same surface coverage and structure is consistent with the similar reductive desorption potentials and indicates that the carboxylate group at this coverage has no significant role in this SAM structure.

The situation is more complex for MBA SAMs formed by immersion of the Au(111) substrate in more concentrated solutions and/or longer t values. In fact, the increase in MBA concentration from 10^{-4} to 10^{-2} M or t from 1 to 24−72 h results in a broader desorption peak located at the same potential but with a larger $q \approx 70-80\ \mu C\ cm^{-2}$ (Figure 2a). On the basis of the reductive desorption curves (Figure 2a), the estimated surface coverage is 0.33, which agrees with that expected for the well-known $c(4 \times 2)$ or the ($\sqrt{3}$ × $\sqrt{3}$)R30° thiol lattices on Au(111). This fact demonstrates that increasing the chemical potential ($\Delta\mu$) of MBA and/or t leads to the formation of a denser layer, as predicted by theoretical calculations and shown in Figure 2b.[36] The broad desorption peak indicates that these dense SAMs are more disordered than the ($\sqrt{3}$ × 4) lattice.[37] In fact, STM images (Figure 2c) show a disordered adlayer, where molecular resolution can not be achieved, which exhibits bright irregular features of different sizes with average height of 0.31/0.35 nm (Figure 2d). We assign these features to MBA aggregates in a second layer placed mostly parallel to the MBA SAM and interacting by hydrogen bonding between carboxylic groups.[37] Interestingly, some vacancy islands (θ_{vac} = 0.08) are now observed on

Figure 2. MBA SAM, $\theta_{MBA} = 0.33$. (a) Electrodesorption curve, (b) γ versus $\Delta\mu_{MBA}$ plots for the $(\sqrt{3} \times 4)$ and $c(4 \times 2)$ MBA lattices on Au(111), (c) $(185 \times 185 \text{ nm}^2)$ STM image, and (d) height histogram for the bright regions in panel c.

terraces (black regions in the STM image), suggesting that the Au(111) surface can reconstruct to form RS-Au$_{ad}$-SR species. In fact, the adatoms provided by this θ_{vac} value plus 0.045 θ_{ad} provided by the lifting of the herringbone reconstruction leads to $\theta_{ad} = 0.125$, a value not far from $\theta_{ad} = 0.165$ required for $\theta_{MBA} = 0.33$ present as RS-Au$_{ad}$-SR. Our results for MBA SAM formed at high concentration and longer t values agree with those reported for MBT.[28] In that work, in addition to the $(\sqrt{3} \times 4)$ lattice, some amount of the dense $c(4 \times 2)$ surface ($\theta_{MBT} = 0.33$) structure was observed, a fact that could justify the formation of vacancy islands and the presence RS-Au$_{ad}$-SR species.

3.1.2. UDT SAMs. In Figure 3a, a typical electrodesorption curve for UDT SAMs on Au(111) is shown. The most important cathodic current peak appears at $E_p = -1.08$ V and involves $q = 75\ \mu C\ cm^{-2}$. This figure is equivalent to a thiolate surface coverage $\theta_{UTD} = 0.33$ characteristic of alkanethiolates on Au(111). One peak occurs at more negative potentials (-1.3 V), which has been also observed for other alkanethiols and is assigned to thiol electrodesorption from surface defects of the gold surface. High resolution STM images reveal that UDT organizes into a $(\sqrt{3} \times \sqrt{3})R30°$ lattice ($\theta_{UTD} = 0.33$) (Figure 3b), a fact consistent with the surface coverage derived from the q value in Figure 3a. This lattice has been repeatedly observed for long chain alkanethiols SAMs on the Au(111) surface.[2,38] STM images of the UDT-covered Au(111) terraces show the typical gold vacancy islands described in alkanethiolate SAMs (dark regions in Figure 3c). As already mentioned, the presence of the vacancy islands have been explained by the formation of RS-Au$_{ad}$-RS species induced by thiol adsorption.

The gold vacancy island coverage θ_{vac} calculated from the analysis of many STM images of UDT SAMs taken on terraces (Figure 3c) results in $\theta_{vac} = 0.11$, a figure close to that has been reported for hexanethiolate and dodecanethiolate SAMs[39] and is regarded as indirect evidence for the presence of RS-Au$_{ad}$-RS moieties. In fact, as already mentioned, the total amount of Au$_{ad}$ for this species considering the maximum thiolate coverage $\theta_{UDT} = 0.33$ is $\theta_{ad} = 0.165$. This coverage can be reached considering the value $\theta_{vac} \approx 0.12$ and additional 0.045 θ_{ad}
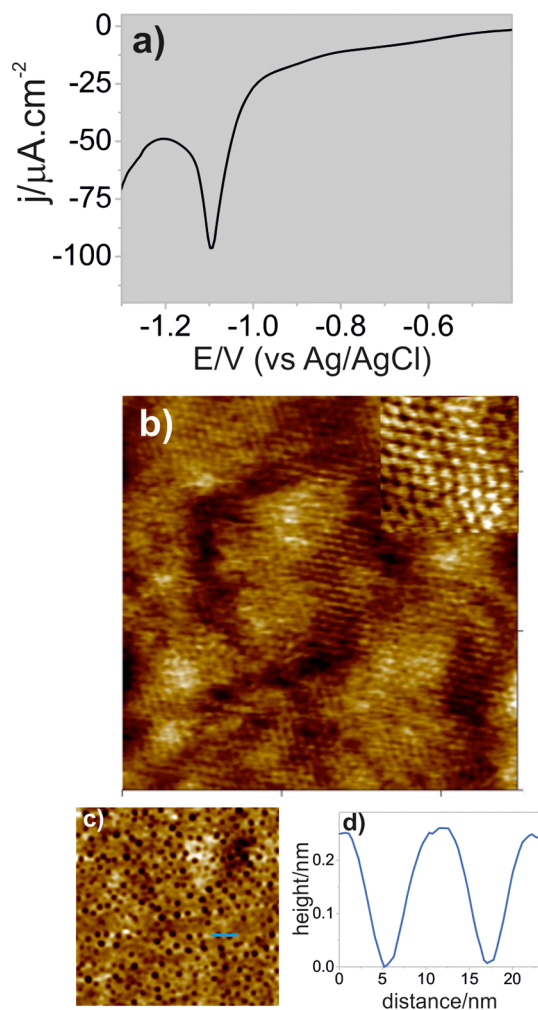
**Figure 3.** UDT SAM. (a) Electrodesorption curve, (b) 25×25 nm^2 STM image, (c) 190×190 nm^2 STM image, and (d) cross section indicated in panel c. The inset in panel b (5×5 nm^2) shows the $(\sqrt{3} \times \sqrt{3})R30°$ lattice.

provided by the lifting of the herringbone reconstruction of the Au(111) surface upon thiol adsorption.[40]

3.1.3. Electronic Properties. The electronic properties of the pure MBA and UDT SAMs were studied by using STS.[41] Figure 4 shows the STS curves for MBA (Figure 4a) and UDT (Figure 4b) SAMs recorded by varying the bias potential (V_{bias}) at a constant tip–sample distance (z), which is controlled by the initial tunneling conditions indicated in the figures. In the case of MBA SAMs, i_t values at the same V_{bias} are greater than those measured through the UDT SAMs, particularly at negative V_{bias}.

The larger i_t values for MBA can be explained by different effects. First, the thickness of MBA SAM is about 0.9 nm smaller than that of UDT, thus facilitating electron tunneling trough the gap.[42] Second, for the same thickness, the molecular conductance of aromatic thiols is 1–2 orders of magnitude larger than the aliphatic thiols.[43] Finally, screening effects arising from the presence of different packing densities ($\theta_{MBA} < \theta_{UDT}$) influence the adsorption-induced charge rearrangements at the metal–molecule interface.[44] This has profound consequences not only for the alignment of the molecular levels with the Fermi energy but also on SAM-induced work-function modification.
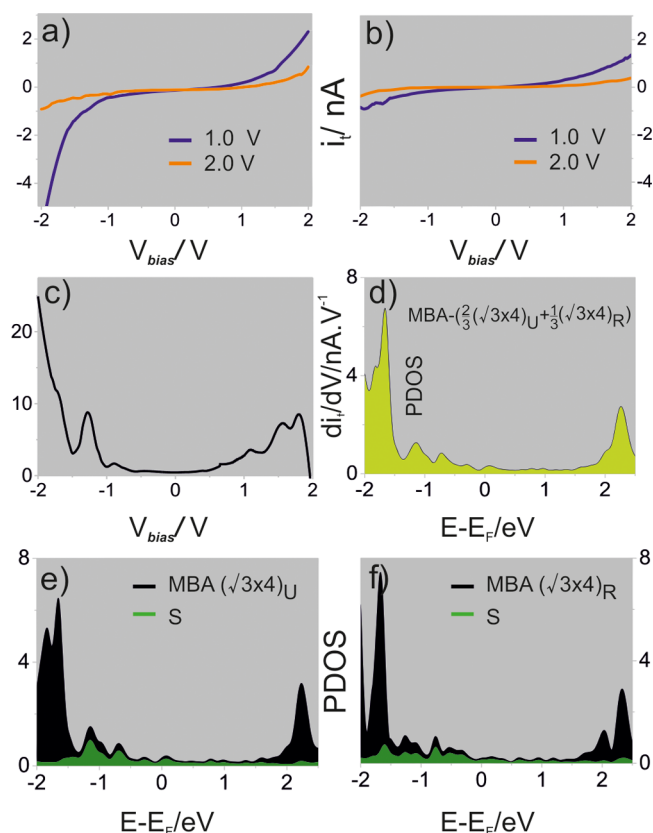
Figure 4. i_t versus V_{bias} curves recorded for (a) MBA and (b) UDT pure SAMs at different potentials (as indicated in the figure); (c) di_t versus dV_{bias} obtained from the i_t versus V_{bias} curves for MBA; (d) density of states projected (PDOS) onto MBA SAMs averaged as 2/3 of unreconstructed and 1/3 of reconstructed ($\sqrt{3} \times 4$) lattice on Au(111); (e) PDOS unreconstructed and (f) reconstructed (staple) ($\sqrt{3} \times 4$) lattice on Au(111) showing the states corresponding to S atom (green curve).

Figure 4c also shows di_t versus dV_{bias} spectrum derived from the i_t versus V_{bias} curves taken on the MBA SAMs. The di_t versus dV_{bias} plot at negative and positive bias voltages probe the filled and empty states of the sample, respectively. Peaks at $\approx -0.8/-1.3$ V and ≈ 1.5 V are observed for MBA SAMs defining a ≈ 2.3 V gap. In UPS measurements on alkanethiolate SAMs with short alkyl chains, small shoulder-like features were recognized at approximately -1.4 eV and were attributed to Au–S bonds localized at the molecule–substrate interface.[45] These peaks are also present in longer chemisorbed thiols on Au(111) such as octanethiol but absent in their physisorbed state.[46] However, similar contributions have been observed in planar aromatic molecules.[47] Therefore, it is not clear the relative contribution of the S and aromatic rings to the MBA molecular conductance at this peak. On the other hand, the states located at $-1.7/-2$ V and at 1.5 V can be assigned to the aromatic ring of the MBA molecule. This point will be discussed in more detail in section 3.3.

3.2. Mixed SAMs. The electrodesorption curves shown in Figures 1 and 2 reveal that the interaction of UDT with Au(111) is stronger than MBA as the UDT peak potential is about 0.4 V more negative than the MBA peak. This fact is reflected in the competitive adsorption of both thiol molecules to the Au(111) surface. In fact, we observed that unless the UDT concentration be set one order of magnitude lower than that of the MBA, UDT species covers immediately the entire

Au(111) surface. Therefore, to produce mixed SAMs the UDT concentration was set at 10^{-4} M while the MBA concentration was progressively increased to 10^{-2} M. Thus, to avoid the formation of the disordered MBA SAM with a large amount of unbounded molecules in a bilayer structure (Figure 2), we use only $t = 1$ h. Under these conditions the surface concentration of UDT and MBA can be controlled to form mixed SAMs.

Figure 5a shows a set of electrodesorption curves recorded in alkaline solutions for mixed SAMs on Au(111) formed by self-assembly from ethanolic solutions with a UDT/MBA concentration ratio (r) varied from $r = 1$ ($10^{-4}:10^{-4}$) to $r =$
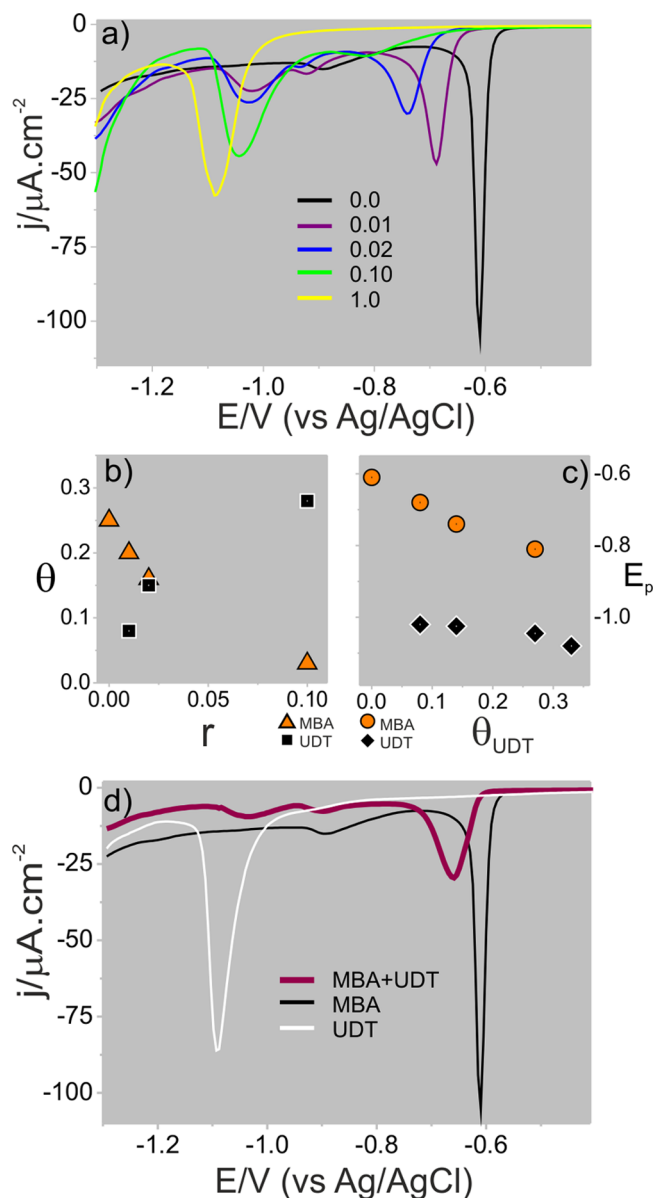
Figure 5. Mixed UDT/MBA SAMs. (a) Electrodesorption curves. The UDT/MBA concentration ratio (r) is indicated. The black line corresponds to a pure MBA SAM used as reference. (b) Dependence of SAM coverage (θ) versus r. (c) Peak potential, E_p, versus UDT surface coverage (θ_{UDT}). (d) Electrodesorption curve corresponding to a MBA SAM prepared from 10^{-4} M MBA and 2 h immersion time after being placed in contact with 10^{-4} M UDT solution for 1 h. The curves corresponding to pure MBA and UDT SAMs are included as reference.

0.01 (10^{-4}:10^{-2}) and $t = 1$ h. We have also included the electrodesorption curve of the pure MBA SAM as reference. The analysis of the desorption curves shown in Figure 5a reveals that as r increases, the θ_{UDT} surface coverage estimated from the q value sharply increases, reaching practically that expected for the complete monolayer at $r = 0.1$ (Figure 5b). Also, the peak shape becomes more defined and the UDT peak potential E_p is negatively shifted, i.e., UDT desorption is more difficult (Figure 5c). At the same time the MBA surface coverage decreases with r (Figure 5b), the MBA peak shape becomes broader (Figure 5a), and the MBA E_p value is markedly shifted in the negative direction (Figure 5c). Note that as r is increased, the total surface coverage (Θ_{total}) changes from 0.25, corresponding to the ordered pure MBA SAM formed at 10^{-4} M, to 0.33, characteristic of a pure UDT SAM.

The shift of E_p for MBA ($\Delta E_p \approx 0.2$ V) and UDT ($\Delta E_p \approx 0.08$ V) as the θ_{UDT} value in mixed SAMs is increased (Figure 5c) reflects stronger vdW interactions between the adsorbed molecules in the mixed SAMs.[48] The large influence of θ_{UDT} on the MBA E_p values should be analyzed considering that MBA desorption takes place from progressively denser and UDT-richer SAMs. In fact, each MBA molecule interacts with more UDT molecules as the θ_{UDT} increases. The shift in E_p reveals that MBA−UDT interactions stabilize the MBA molecules and introduces an additional energy barrier for its electrodesorption, which becomes progressively more difficult.[49] The broader MBA peak also reflects the existence of MBA−UDT interactions. In contrast, the desorption of UDT molecules takes places after complete MBA removal from the surface; therefore, the negative shift of E_p with increasing θ_{UDT} results from more UDT−UDT interactions on the Au(111) surface.

On the other hand, when well-ordered MBA SAMs (Figure 1) are placed in contact with a solution containing 10^{-4} M UDT molecules, the MBA replacement by UDT proceeds slowly. In fact, after 1 h, the amount of UDT incorporated into the MBA SAM is too small, as reflected by the charge density involved in its desorption peak at ≈ -1.0 V (Figure 5d). However, the incorporation of a few UDT molecules into the MBA SAM has a pronounced effect in the MBA peak shape and position as it becomes broader and is shifted toward more negative values. A complete removal of MBA by the UDT molecules requires $t = 24$ h. The fact that competitive adsorption to form a rich UDT surface is much faster (Figure 5a−c) than ligand replacement (Figure 5d) indicates that the ordered MBA SAMs shown in Figure 1 are very stable.[37] The most likely explanation for this is that in the competitive adsorption the larger UDT molecules displace the small MBA molecules in the initial physisorbed stage, whereas in ligand replacement UDT molecules need to break the strong S head−Au bonds of the MBA SAM.

Figure 6a shows the voltammogram and STM images corresponding to a sample where the charge density involved in the reductive desorption of each thiol is practically the same, being $q = 32.1$ μC/cm^2 for UDT and $q = 34.7$ μC/cm^2 for MBA. These figures correspond to $\Theta \approx 0.31$ resulting from $\theta_{MBA} \approx 0.14$ and $\theta_{UDT} \approx 0.17$. The absence of vacancy islands can be observed as well in Figure 6b,c.

The cross section analysis (Figure 6d) of the dark regions shown in Figure 6c indicates that they are shallow, ≈ 0.07 nm in depth, a value far from that expected for vacancy islands (0.24 nm, see cross section in Figure 3c). Thus, the height difference could result from randomly distributed domains of MBA and UDT molecules. Taking into account geometric
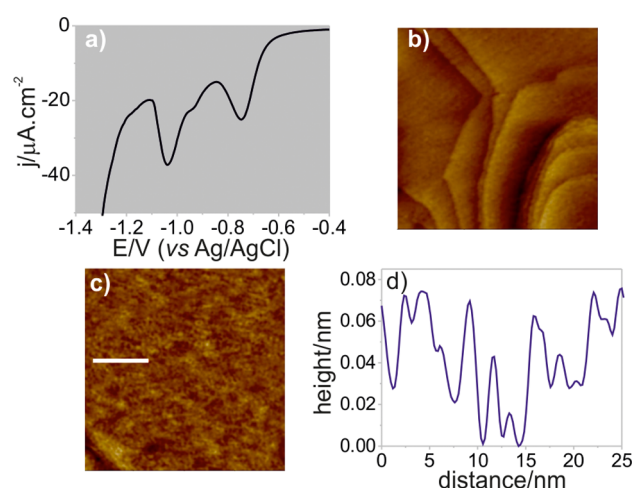

Figure 6. Mixed SAM with $\theta_{MBA} \approx \theta_{UDT}$. (a) Electrodesorption curve; (b) STM image 300 × 300 nm^2; (c) STM image 100 × 100 nm^2; and (d) cross section indicated as a white line in panel c.

considerations, we expect ≈ 0.8 nm, a much greater height difference assuming the same tilt angle. However, it is well-known that topography is convoluted with electronic effects in STM imaging. In fact, the STS curves (Figure 4a,b) show that molecular conductance of MBA is greater than that of UDT, thus compensating the geometric difference and resulting in much smaller apparent height differences in the STM images. The formation of MBA domains in mixed MBA−alkanethiolate SAMs has also been revealed by surface-enhanced Raman spectroscopy.[50] Note that there are not ordered regions in the mixed SAM and molecular resolution can not be achieved. The absence of vacancy islands is an important feature of these mixed SAMs. They are recovered by increasing the θ_{UDT} coverage ($\theta_{UDT} > 0.3$) at the Au surface.

We have tested the ability of MBA molecules to wire the charge transfer from the $[Fe(CN)_6]^{4-}/[Fe(CN)_6]^{3-}$ redox couple in solution to the Au(111) substrate covered by the non-conductive UDT SAM. For this purpose we have prepared a UDT-rich SAM ($r = 0.05$) containing a small amount of MBA molecules and compared the behavior of the redox couple with those observed for the pure UDT and MBA SAMs.

Figure 7 shows the blocking properties of UDT SAMs due to the presence of a thick, ordered, and hydrophobic aliphatic barrier that hinders electroactive species to be close to the Au(111) surface.[51] Therefore, electron transfer is difficult and highly irreversible on these surfaces.[52] In contrast, MBA SAMs are thinner and have a lower coverage, allowing a better
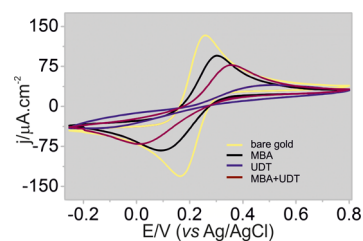
Figure 7. Voltammogram curves showing the electrochemical response of 1 mM $[Fe(CN)_6]^{4-}/[Fe(CN)_6]^{3-}$ + 0.1 M KNO$_3$ aqueous solution for bare gold (yellow), pure MBA SAM (black), mixed SAM formed using $r = 0.05$ and immersion time of 1 h (red), and pure UDT SAM (blue).

30018

dx.doi.org/10.1021/jp510398m | J. Phys. Chem. C 2014, 118, 30013−30022

approximation of the electroactive species to the metallic surface (Figure 7). Moreover, π electrons present in the aromatic ring and relatively close to the Au surface (see the tilt angle values, α in Table 1) contribute in the charge transfer

**Table 1. Energetic and Structural Data for MBA Surface Structures on Au(111)**

surface lattice	energetic and structural data		
	$(\sqrt{3} \times 4)$		$c(4 \times 2)$
θ_{MBA}	1/4	1/4	1/3
$\theta_{Au\ adatom}$	0.0	1/8	1/6
E_b (eV)	−2.56	−2.92	−3.05
E_{rec}/N_{thiol} (eV)	0.00	+0.42	+0.56
$E_b + E_{rec}/N_{MBA}$ (eV)	−2.56	−2.50	−2.49
γ (eV Å^{-2})	−0.085	−0.084	−0.111
S Bader charge (e)	−0.11	−0.11	−0.13
Au Bader charge (e)	+0.02	+0.15[a] 0.0	+0.21[a] 0.0
tilt angle, α (deg)	46.1	45.6	29.0

[a]Au adatom.

process in agreement with the better molecular conductance shown in the STS curves (Figure 4). On the other hand, the mixed SAM prepared at $r = 0.05$ and $t = 1$ h, which contains a small amount of conductive MBA molecules embedded in the UDT SAM, efficiently wire the electroactive species with the Au surface, markedly improving the reversibility of the redox couple. It means that even a small amount of MBA molecules in an aliphatic thiol are able to improve electron transfer. Our experimental data supports previous findings related to mixed SAMs.[53,54]

3.3. DFT Results. This section is focused on answering theoretically relevant questions resulting from our experimental results. First, we should explain the absence of vacancy islands in the MBA ($\sqrt{3} \times 4$) surface structure (Figure 1b). Our DFT calculations (Table 1) show that the MBA binding energy in the ($\sqrt{3} \times 4$) surface structure containing RS-Au$_{ad}$-SR species is stronger than that in the same lattice formed by MBA* radicals. However, as already discussed, the binding energy is not the unique criterion that must be taken into account to predict the stability of the different surface structures because it does not consider the energy cost to reconstruct the Au(111) surface, i.e., the energy required to remove the Au adatoms needed to form the RS-Au$_{ad}$-SR moieties. Therefore, to estimate the stability of the ($\sqrt{3} \times 4$) lattices formed by either MBA* or RS-Au$_{ad}$-SR shown in Figure 8 we have compared the two energetic terms per thiol adsorbed: on one hand, the cost to form the reconstructed surface, E_{rec}/N_{MBA}, and on the other hand, the gain of stability when one thiol binds to the surface, E_b. Therefore, the energetic balance per adsorbed thiol on both surface structures should be estimated as $E_b + E_{rec}/N_{MBA}$. Results from these calculations (Table 1) indicate that the ($\sqrt{3} \times 4$) lattice formed by MBA* radicals on the unreconstructed Au(111) surface is slightly more stable than the same lattice formed by RS-Au$_{ad}$-SR moieties, thus justifying the absence of pits on the Au(111) terraces.

Another interesting question concerns the stability of the ($\sqrt{3} \times 4$) lattice. The ($\sqrt{3} \times 4$) lattice dominates in diluted solutions or short t values, whereas dense SAMs are formed in concentrated solutions or much longer time, as shown in Figures 1 and 2. On the other hand, these dense SAMs are compatible with ($\sqrt{3} \times \sqrt{3}$)R30° or $c(4 \times 2)$ lattices. We have already shown[55] that to compare the stability of surface
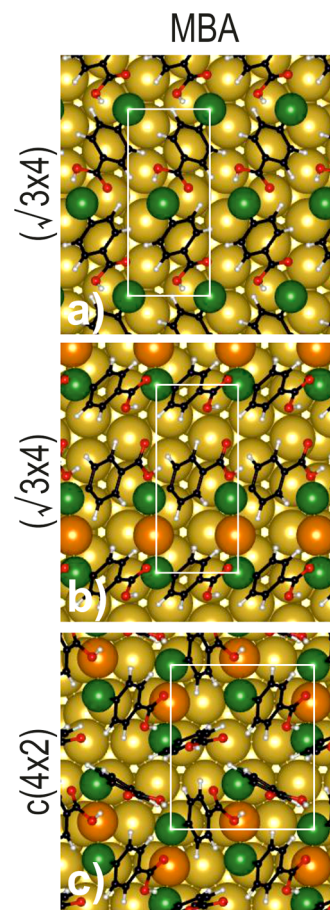
Figure 8. Optimized MBA surface structures on Au(111): (a) unreconstructed ($\sqrt{3} \times 4$); (b) reconstructed ($\sqrt{3} \times 4$); and (c) reconstructed $c(4 \times 2)$. Green, S; black, C; white, H; red, Au adatom; yellow, Au. The corresponding unit cells are drawn on the figures.

structure with different coverage and lattice constants, the calculation of the corresponding γ values is needed.

The γ versus chemical potential plot ($\Delta\mu_{MBA}$) for the ($\sqrt{3} \times 4$) lattice formed by the MBA* adsorbates and for the $c(4 \times 2)$ lattice formed by RS-Au$_{ad}$-SR moieties is shown in Figure 2b. This plot predicts ($\sqrt{3} \times 4$) to stapple-containing $c(4 \times 2)$ lattice transition as $\Delta\mu_{MBA}$ is increased and accordingly the presence of vacancy islands at terraces in concentrated MBA solutions (Figure 2c). Note that this transition involves a change in the tilt angle from $\alpha = 45°$ to 29° that reflects a weaker aromatic ring–Au substrate and stronger aromatic ring–aromatic ring interactions. An additional factor that could contribute to the formation of a dense layer at high $\Delta\mu_{MBA}$ is the formation of the MBA bilayer by hydrogen bonding, but this contribution is not present in our DFT calculations.

Another intriguing feature is the absence of vacancy islands when the surface is covered by equivalent amounts of the MBA and UDT ($\theta_{MBA} = \theta_{UDT} = 0.16$). To answer this question we need to assume that the surface structures for the ($\sqrt{3} \times 4$) MBA and ($\sqrt{3} \times \sqrt{3}$)R30° UDT lattices observed in the STM images are still valid for the mixed SAMs. First, we should remember that the ($\sqrt{3} \times 4$)-MBA SAM is formed by MBA* adsorbates; therefore, it does not produce vacancy islands. The situation is different for the UDT SAMs where vacancy islands are a fingerprint of alkanethiol adsorption. We use the ($3\sqrt{3} \times 3\sqrt{3}$)R30° alkanethiolate lattice model for this SAM because it is consistent with the ($\sqrt{3} \times \sqrt{3}$)R30° STM images and also

30019

dx.doi.org/10.1021/jp510398m | J. Phys. Chem. C 2014, 118, 30013−30022

with the vacancy island coverage experimentally observed.[56] In fact, the $(3\sqrt{3} \times 3\sqrt{3})R30°$- UDT lattice needs a Au_{ad} per three adsorbed thiols as $RS\text{-}Au_{ad}\text{-}SR + RS^*$. Taking into account that the surface coverage of UDT is $\theta_{UDT} \approx 0.16 = 1/6$ in this mixed SAM, we need $\theta_{ad} = 0.055$ to form the $RS\text{-}Au_{ad}\text{-}SR$ species in the $(3\sqrt{3} \times 3\sqrt{3})R30°$ lattice ($\theta_{ad} = 1/3 \times 1/6 = 0.055$). This quantity could be provided by the lifting of the herringbone reconstruction ($\theta_{ad} = 0.045$), i.e., no additional source of adatoms is needed, and then no significant amount of vacancy islands can be observed.

The difference in E_p values for the pure and MBA and UDT SAMs should also be considered in terms of SAM stability. The reductive desorption of thiol SAMs from the Au(111) surface involves a nucleation and growth of thiol-free regions on the Au surface.[57] Therefore, we could consider the energetic difference in stability of a MBA moiety in the $(\sqrt{3} \times 4)$ lattice with respect to a UDT moiety in a $(3\sqrt{3} \times 3\sqrt{3})R30°$ environment as a qualitative estimation of the E_p behavior. In principle, this difference could be roughly estimated from the E_b+E_{rec}/N_{thiol} MBA value (Table 1) that is significantly less negative than those estimated for long alkanethiolates,[56] thus explaining the easier desorption of the MBA molecules from the Au(111) surface.

Finally, the calculated PDOS for the MBA lattices (Figure 4d−f) are compared to the experimental di_t versus dV_{bias} plots in Figure 4c. For the calculated $(\sqrt{3} \times 4)$ unreconstructed MBA lattice (Figure 4e), the HOMO appears at −0.7 eV with a close state at −1.2 eV. In both cases, the principal contribution arises from S states. These states can be efficient channels for conduction at low V_{bias}. Other prominent states, which arise mainly from C, H, and O states of the adsorbate, are visible at −1.7 eV. While the HOMO and the deeper states are in good agreement with the experimental ones, the estimated LUMO value (2.2 V) is about 0.7 eV more positive than the observed value in the experimental STS data (Figure 4c). On the other hand, the PDOS for the $(\sqrt{3} \times 4)$ reconstructed lattice MBA consisting of $RS\text{-}Au_{ad}\text{-}SR$ species (Figure 4f) also exhibits the HOMO at −0.7 eV. At −1.7 eV, a sharp peak also appears, but in this case not only the S states but also the C, H, and O states of the molecule contribute. In this case, the LUMO is observed at 2.0 V, a value closer to that observed in the experiment. In both lattices, S states are broadened by the interaction with the Au surface states in the region close to the Fermi level. Considering that the unreconstructed lattice (MBA*) should also contain $RS\text{-}Au_{ad}\text{-}SR$ species resulting from the lifting of the herringbone reconstruction, which provides 0.045 Au_{ad} and accordingly double number of thiolates, 0.09, we have estimated the PDOS for a system consisting of 2/3 unreconstructed and 1/3 of reconstructed lattices (Figure 4d), which is in excellent agreement with the experimental data (Figure 4c). The structure of the filled states can explain the large negative i_t values in the STS curves in comparison with alkanethiolates. In fact, our calculations reveal that delocalized states of the aromatic ring are located at −1.7 eV below E_f whereas similar states for alkanethiolate chains are about −3/−4 eV below E_f.[46,58] Therefore, PDOS structure justifies the better molecular conductance of MBA SAMs in relation to alkanethiolates SAMs.

4. CONCLUSIONS

We have confirmed that MBA forms an ordered diluted $(\sqrt{3} \times 4)$ lattice on Au(111) without evidence of Au adatom complex formation at terraces (absence of vacancy islands) at low MBA concentrations, a fact consistent with the similar surface free energy of this lattice formed by either MBA radicals or MBA−Au_{ad} complexes. In contrast, we have found denser and disordered lattices with vacancy island formation at high MBA concentrations, suggesting the presence of Au adatom complexes in agreement with results observed in MBA-capped Au nanoclusters.[59] Also, MBA bilayers are formed under these conditions that contribute to the surface disorder. The electrochemical stability of MBA molecules is markedly improved in mixed MBA−UDT SAMs revealing aromatic−aliphatic attractive interactions. The mixed SAMs at equivalent amounts of thiols do not exhibit vacancy island formation, which is typical of the pure UDT SAMs, a fact that can be explained in terms of surface models. The MBA SAMs exhibit good molecular conductance at negative V_{bias} because of the presence of filled S and aromatic ring states near the Fermi level. Finally, and in concordance with the above results, it has been proven that MBA molecules efficiently wire the electron transfer through UDT SAMs.

■ AUTHOR INFORMATION

Corresponding Author
*Tel: +34 922318021. E-mail: ahcreus@ull.es.

Notes
The authors declare no competing financial interest.

■ REFERENCES

(1) Ulman, A. Formation and Structure of Self-Assembled Monolayers. *Chem. Rev. (Washington, DC, U.S.)* **1996**, *96*, 1533−1554.
(2) Vericat, C.; Vela, M. E.; Benitez, G.; Carro, P.; Salvarezza, R. C. Self-Assembled Monolayers of Thiols and Dithiols on Gold: New Challenges for a Well-Known System. *Chem. Soc. Rev.* **2010**, *39*, 1805−1834.
(3) Maksymovych, P.; Voznyy, O.; Dougherty, D. B.; Sorescu, D. C.; Yates, J. T., Jr. Gold Adatom as a Key Structural Component in Self-Assembled Monolayers of Organosulfur Molecules on Au(1 1 1). *Prog. Surf. Sci.* **2010**, *85*, 206−240.
(4) Guo, Q.; Li, F. Self-Assembled Alkanethiol Monolayers on Gold Surfaces: Resolving the Complex Structure at the Interface by STM. *Phys. Chem. Chem. Phys.* **2014**, *16* (36), 19074−19090.
(5) Love, J. C.; Estroff, L. A.; Kriebel, J. K.; Nuzzo, R. G.; Whitesides, G. M. Self-Assembled Monolayers of Thiolates on Metals as a Form of Nanotechnology. *Chem. Rev. (Washington, DC, U.S.)* **2005**, *105*, 1103−1169.
(6) Kind, M.; Wöll, C. Organic Surfaces Exposed by Self-Assembled Organothiol Monolayers: Preparation, Characterization, and Application. *Prog. Surf. Sci.* **2009**, *84*, 230−278.
(7) Bain, C. D.; Evall, J.; Whitesides, G. M. Formation of Monolayers by the Coadsorption of Thiols on Gold: Variation in the Head Group, Tail Group, and Solvent. *J. Am. Chem. Soc.* **1989**, *111*, 7155−7164.
(8) Bain, C. D.; Whitesides, G. M. Formation of Monolayers by the Coadsorption of Thiols on Gold: Variation in the Length of the Alkyl Chain. *J. Am. Chem. Soc.* **1989**, *111*, 7164−7175.
(9) Hobara, D.; Sasaki, T.; Imabayashi, S.; Kakiuchi, T. Surface Structure of Binary Self-Assembled Monolayers Formed by Electrochemical Selective Replacement of Adsorbed Thiols. *Langmuir* **1999**, *15*, 5073−5078.

(10) González-Granados, Z.; Sánchez-Obrero, G.; Madueño, R.; Sevilla, J. M.; Blázquez, M.; Pineda, T. Formation of Mixed Monolayers from 11-Mercaptoundecanoic Acid and Octanethiol on Au(111) Single Crystal Electrode Under Electrochemical Control. *J. Phys. Chem. C* **2013**, *117*, 24307–24316.

(11) Wong, E. H. J.; May, G. L.; Wilde, C. P. Oxidative Desorption of Thiols as a Route to Controlled Formation of Binary Self Assembled Monolayer Surfaces. *Electrochim. Acta* **2013**, *109*, 67–74.

(12) Kakiuchi, T.; Iida, M.; Gon, N.; Hobara, D.; Imabayashi, S.; Niki, K. Miscibility of Adsorbed 1-Undecanethiol and 11-Mercaptoundecanoic Acid Species in Binary Self-Assembled Monolayers on Au(111). *Langmuir* **2001**, *17*, 1599–1603.

(13) Hobara, D.; Ota, M.; Imabayashi, S.; Niki, K.; Kakiuchi, T. Phase Separation of Binary Self-Assembled Thiol Monolayers Composed of 1-Hexadecanethiol and 3-Mercaptopropionic Acid on Au(111) Studied by Scanning Tunneling Microscopy and Cyclic Voltammetry. *J. Electroanal. Chem.* **1998**, *444*, 113–119.

(14) Donten, M. L.; Królikowska, A.; Bukowska, J. Structure and Composition of Binary Monolayers Self-Assembled from Sodium 2-Mercaptoetanosulfonate and Mercaptoundecanol Mixed Solutions on Silver and Gold Supports. *Phys. Chem. Chem. Phys.* **2009**, *11*, 3390–3400.

(15) Poirier, G. E. Characterization of Organosulfur Molecular Monolayers on Au(111) using Scanning Tunneling Microscopy. *Chem. Rev. (Washington, DC, U.S.)* **1997**, *97*, 1117–1127.

(16) Schaefer, A. H.; Seidel, C.; Chi, L.; Fuchs, H. STM Investigations of Thiol Self-Assembled Monolayers. *Adv. Mater. (Weinheim, Ger.)* **1998**, *10*, 839–842.

(17) Sawaguchi, T.; Sato, Y.; Mizutani, F. In Situ STM Imaging of Individual Molecules in Two-Component Self-Assembled Monolayers of 3-Mercaptopropionic Acid and 1-Decanethiol on Au(111). *J. Electroanal. Chem.* **2001**, *496*, 50–60.

(18) Chen, S.; Li, L.; Boozer, C. L.; Jiang, S. Controlled Chemical and Structural Properties of Mixed Self-Assembled Monolayers of Alkanethiols on Au(111). *Langmuir* **2000**, *16*, 9287–9293.

(19) Horcas, I.; Fernández, R.; Gómez-Rodríguez, J. M.; Colchero, J.; Gómez-Herrero, J.; Baro, A. M. WSXM: A Software for Scanning Probe Microscopy and a Tool for Nanotechnology. *Rev. Sci. Instrum.* **2007**, *78*.

(20) Kresse, G.; Hafner, J. Ab Initio Molecular Dynamics for Open-Shell Transition Metals. *Phys. Rev. B: Condens. Matter Mater. Phys.* **1993**, *48*, 13115–13118.

(21) Kresse, G.; Furthmüller, J. Efficiency of Ab-Initio Total Energy Calculations for Metals and Semiconductors using a Plane-Wave Basis Set. *Comput. Mater. Sci.* **1996**, *6*, 15–50.

(22) Dion, M.; Rydberg, H.; Schröder, E.; Langreth, D. C.; Lundqvist, B. I. Van Der Waals Density Functional for General Geometries. *Phys. Rev. Lett.* **2004**, *92*, 246401–1.

(23) Klimeš, J.; Bowler, D. R.; Michaelides, A. Chemical Accuracy for the Van Der Waals Density Functional. *J. Phys.: Condens. Matter* **2010**, *22*.

(24) Blöchl, P. E. Projector Augmented-Wave Method. *Phys. Rev. B: Condens. Matter Mater. Phys.* **1994**, *50*, 17953–17979.

(25) Monkhorst, H. J.; Pack, J. D. Special Points for Brillouin-Zone Integrations. *Phys. Rev. B: Condens. Matter Mater. Phys.* **1976**, *13*, 5188–5192.

(26) Pearson, W. B. In *Handbook of Lattice Spacing and Structure of Metals*; Pergamon Press, Inc.: New York, 1958.

(27) Arihara, K.; Ariga, T.; Takashima, N.; Arihara, K.; Okajima, T.; Kitamura, F.; Tokuda, K.; Ohsaka, T. Multiple Voltammetric Waves for Reductive Desorption of Cysteine and 4-Mercaptobenzoic Acid Monolayers Self-Assembled on Gold Substrates. *Phys. Chem. Chem. Phys.* **2003**, *5*, 3758–3761.

(28) Seo, K.; Borguet, E. Potential-Induced Structural Change in a Self-Assembled Monolayer of 4-Methylbenzenethiol on Au(111). *J. Phys. Chem. C* **2007**, *111*, 6335–6342.

(29) Pensa, E.; Rubert, A. A.; Benitez, G.; Carro, P.; Orive, A. G.; Creus, A. H.; Salvarezza, R. C.; Vericat, C. Are 4-Mercaptobenzoic Acid Self Assembled Monolayers on Au(111) a Suitable System to Test Adatom Models? *J. Phys. Chem. C* **2012**, *116*, 25765–25771.

(30) Liu, Y.; Lee, Y. Adsorption Characteristics of OH-Terminated Alkanethiol and Arenethiol on Au(111) Surfaces. *Nanoscale* **2012**, *4*, 2093–2100.

(31) Li, F.; Tang, L.; Voznyy, O.; Gao, J.; Guo, Q. The Striped Phases of Ethylthiolate Monolayers on the Au(111) Surface: A Scanning Tunneling Microscopy Study. *J. Chem. Phys.* **2013**, *138*.

(32) Tang, L.; Li, F.; Zhou, W.; Guo, Q. The Structure of Methylthiolate and Ethylthiolate Monolayers on Au(111): Absence of the $(\sqrt{3} \times \sqrt{3})R30°$ Phase. *Surf. Sci.* **2012**, *606*, L31–L35.

(33) Hagenström, H.; Schneeweiss, M. A.; Kolb, D. M. Modification of a Au(111) Electrode with Ethanethiol. 1. Adlayer Structure and Electrochemistry. *Langmuir* **1999**, *15*, 2435–2443.

(34) Zhang, J.; Chi, Q.; Ulstrup, J. Assembly Dynamics and Detailed Structure of 1-Propanethiol Monolayers on Au(111) Surfaces Observed Real Time by in Situ STM. *Langmuir* **2006**, *22*, 6203–6213.

(35) Wang, Y.; Chi, Q.; Hush, N. S.; Reimers, J. R.; Zhang, J.; Ulstrup, J. Gold Mining by Alkanethiol Radicals: Vacancies and Pits in the Self-Assembled Monolayers of 1-Propanethiol and 1-Butanethiol on Au(111). *J. Phys. Chem. C* **2011**, *115*, 10630–10639.

(36) Azcárate, J. C.; Corthey, G.; Pensa, E.; Vericat, C.; Fonticelli, M. H.; Salvarezza, R. C.; Carro, P. Understanding the Surface Chemistry of Thiolate-Protected Metallic Nanoparticles. *J. Phys. Chem. Lett.* **2013**, *4*, 3127–3138.

(37) Lee, J. R. I.; Willey, T. M.; Nilsson, J.; Terminello, L. J.; De Yoreo, J. J.; Van Buuren, T. Effect of Ring Substitution Position on the Structural Conformation of Mercaptobenzoic Acid Self-Assembled Monolayers on Au(111). *Langmuir* **2006**, *22*, 11134–11141.

(38) Vericat, C.; Vela, M. E.; Salvarezza, R. C. Self-Assembled Monolayers of Alkanethiols on Au(111): Surface Structures, Defects and Dynamics. *Phys. Chem. Chem. Phys.* **2005**, *7*, 3258–3268.

(39) Pensa, E.; Cortés, E.; Corthey, G.; Carro, P.; Vericat, C.; Fonticelli, M. H.; Benítez, G.; Rubert, A. A.; Salvarezza, R. C. The Chemistry of the Sulfur-Gold Interface: In Search of a Unified Model. *Acc. Chem. Res.* **2012**, *45*, 1183–1192.

(40) Grönbeck, H.; Häkkinen, H.; Whetten, R. L. Gold–Thiolate Complexes Form a Unique $c(4 \times 2)$ Structure on Au(111). *J. Phys. Chem. C* **2008**, *112*, 15940–15942.

(41) Jäckel, F.; Rabe, J. P. In *Scanning Probe Microscopies Beyond Imaging*; Samorì, P., Ed.; WILEY-VCH: Weinheim, Germany, 2006.

(42) Wold, D. J.; Haag, R.; Rampi, M. A.; Frisbie, C. D. Distance Dependence of Electron Tunneling through Self-Assembled Monolayers Measured by Conducting Probe Atomic Force Microscopy: Unsaturated Versus Saturated Molecular Junctions. *J. Phys. Chem. B* **2002**, *106*, 2813–2816.

(43) DiBenedetto, S. A.; Facchetti, A.; Ratner, M. A.; Marks, T. J. Molecular Self-Assembled Monolayers and Multilayers for Organic and Unconventional Inorganic Thin-Film Transistor Applications. *Adv. Mater. (Weinheim, Ger.)* **2009**, *21*, 1407–1433.

(44) Toerker, M.; Fritz, T.; Proehl, H.; Gutierrez, R.; Großmann, F.; Schmidt, R. Electronic Transport through Occupied and Unoccupied States of an Organic Molecule on Au: Experiment and Theory. *Phys. Rev. B: Condens. Matter Mater. Phys.* **2002**, *65*, 2454221–2454228.

(45) Alloway, D. M.; Hofmann, M.; Smith, D. L.; Gruhn, N. E.; Graham, A. L.; Colorado, R., Jr.; Wysocki, V. H.; Lee, T. R.; Lee, P. A.; Armstrong, N. R. Interface Dipoles Arising from Self-Assembled Monolayers on Gold: UV-Photoemission Studies of Alkanethiols and Partially Fluorinated Alkanethiols. *J. Phys. Chem. B* **2003**, *107*, 11690–11699.

(46) Nakaya, M.; Shikishima, M.; Shibuta, M.; Hirata, N.; Eguchi, T.; Nakajima, A. Molecular-Scale and Wide-Energy-Range Tunneling Spectroscopy on Self-Assembled Monolayers of Alkanethiol Molecules. *ACS Nano* **2012**, *6*, 8728–8734.

(47) Lei, S.; De Feyter, S. STM, STS and Bias-Dependent Imaging on Organic Monolayers at the Solid-Liquid Interface. *Top. Curr. Chem.* **2008**, *285*, 269–312.

(48) Kakiuchi, T.; Usui, H.; Hobara, D.; Yamamoto, M. Voltammetric Properties of the Reductive Desorption of Alkanethiol

Self-Assembled Monolayers from a Metal Surface. *Langmuir* **2002**, *18*, 5231−5238.

(49) Hobara, D.; Ueda, K.; Imabayashi, S.; Yamamoto, M.; Kakiuchi, T. Phase Separation of Binary Self-Assembled Thiol Monolayers of 2-Mercaptoethanesulfonic Acid and 1-Octadecanethiol on Au(111). *Electrochemistry (Tokyo, Jpn.)* **1999**, *67*, 1218−1220.

(50) Urcuyo, R.; Cortés, E.; Rubert, A. A.; Benitez, G.; Montero, M. L.; Tognalli, N. G.; Fainstein, A.; Vela, M. E.; Salvarezza, R. C. Aromatic and Aliphatic Thiol Self-Assembled Monolayers on Au: Anchoring and Delivering Copper Species. *J. Phys. Chem. C* **2011**, *115*, 24707−24717.

(51) Porter, M. D.; Bright, T. B.; Allara, D. L.; Chidsey, C. E. D. Spontaneously Organized Molecular Assemblies. 4. Structural Characterization of *n*-Alkyl Thiol Monolayers on Gold by Optical Ellipsometry, Infrared Spectroscopy, and Electrochemistry. *J. Am. Chem. Soc.* **1987**, *109*, 3559−3568.

(52) Miller, C.; Cuendet, P.; Grätzel, M. Adsorbed ω-Hydroxy Thiol Monolayers on Gold Electrodes: Evidence for Electron Tunneling to Redox Species in Solution. *J. Phys. Chem.* **1991**, *95*, 877−886.

(53) Noh, J.; Park, H.; Jeong, Y.; Kwon, S. Structure and Electrochemical Behavior of Aromatic Thiol Self-Assembled Monolayers on Au(111). *Bull. Korean Chem. Soc.* **2006**, *27*, 403−406.

(54) Coelho, D.; Machado, S. A. S. New Contribution in the Study of Phase Formation in Mixed Alkanethiol Self-Assembled Monolayers: A Powerful Tool for Transducers Design. *Electrochim. Acta* **2014**, *142*, 191−201.

(55) Torres, D.; Carro, P.; Salvarezza, R. C.; Illas, F. Evidence for the Formation of Different Energetically Similar Atomic Structures in Ag(111)-($\sqrt{7} \times \sqrt{7}$)-R19.1°-CH₃S. *Phys. Rev. Lett.* **2006**, *97*.

(56) Carro, P.; Torrelles, X.; Salvarezza, R. C. A Novel Model for the ($\sqrt{3} \times \sqrt{3}$)R30° Alkanethiolate-Au(111) Phase Based on Alkanethiolate-Au Adatom Complexes. *Phys. Chem. Chem. Phys.* **2014**, *16*, 19017−19023.

(57) Martin, H.; Vericat, C.; Andreasen, G.; Vela, M. E.; Salvarezza, R. C. A Monte Carlo Simulation for the Stripping of the $\sqrt{3} \times \sqrt{3}$ R30° Alkanethiol Lattice from Au(111) Terraces and Steps. *J. Chem. Phys.* **2002**, *117*, 2293−2298.

(58) Seminario, J. M.; Yan, L. Ab Initio Analysis of Electron Currents in Thioalkanes. *Int. J. Quantum Chem.* **2005**, *102*, 711−723.

(59) Jadzinsky, P. D.; Calero, G.; Ackerson, C. J.; Bushnell, D. A.; Kornberg, R. D. Structure of a Thiol Monolayer-Protected Gold Nanoparticle at 1.1 Å Resolution. *Science* **2007**, *318*, 430−433.